This is the authors' version of the article published in Macromolecules. Changes were made to this version by the publisher prior to publication. The final version is available at 10.1021/acs.macromol.4c02894

Advancing non-isocyanate polyurethane foams: exo-vinylene cyclic carbonate–amine chemistry enabling room-temperature reactivity and fast self-blowing

Maksim Makarov[1], Maxime Bourguignon[1], Bruno Grignard[1,2]*, Christophe Detrembleur[1,3]*

[1]Center for Education and Research on Macromolecules (CERM), CESAM Research Unit, University of Liege, Sart-Tilman B6a, 4000 Liege, Belgium

[2]FRITCO$_2$T Platform, University of Liege, Sart-Tilman B6a, 4000 Liege, Belgium

[3]WEL Research Institute, avenue Pasteur, 6, 1300 Wavre, Belgium

* Corresponding authors: **E-mail:** Bruno.Grignard@uliege.be; Christophe.Detrembleur@uliege.be.

Abstract.

Though widely used, polyurethane foams raise health concerns stemming from their isocyanate precursors. Non-isocyanate polyurethane foams (NIPUFs), synthesized by aminolysis of 5-membered cyclic carbonates, represent safer and more sustainable alternatives. Despite their potential, achieving efficient self-blowing NIPUFs from room temperature (RT) formulations has proven highly challenging, as previous methods rely on external heat sources, prolonged reaction times, or are based on hybrid formulations involving epoxides. In this study, we demonstrate a new concept that makes rapid the production of full NIPUFs (i.e., with exclusive urethane linkages) from RT solvent-free formulations through the incorporation of exo-vinylene cyclic carbonate (αCC). This approach incorporated hydroxyoxazolidone groups, i.e., cyclic hydroxyurethanes, as pendant groups of the polyhydroxyurethane backbone. We investigated the reactions occurring in this foaming system and identified optimal foaming formulations to rapidly produce the foams within 1 – 5 minutes, with a high gel content. The study explored monomer variations as amine mixtures and different αCCs. Compression tests revealed

that the foam's mechanical properties were easily tuned by adapting the formulation composition, giving access to both flexible and rigid foams with pore sizes in the range of conventional PU foams. Moreover, we highlighted the importance of the hydrophilic nature of NIPUFs on their mechanical properties, with a decrease in the Young's modulus when exposed to increased humidity contents. While these foams, like many NIPUs, exhibit inherent hydrophilicity, this limitation may be addressed through additives or future formulation optimization. Our new concept paves the way for the rapid preparation of the next generation of full isocyanate-free polyurethane foams with modular properties.

1. Introduction.

Polyurethanes (PUs) play a significant role in the global foam market due to their easily modifiable chemical, physical, and mechanical properties[1,2]. Conventional PU foams are produced by a step-growth polyaddition reaction between phosgene-derived poly(isocyanate) and polyol monomers, while the foaming process exploits CO_2 as an internal blowing agent, generated via isocyanate hydrolysis[3,4]. However, the fossil origin and toxic nature of isocyanates, combined with limited viable recycling scenarios of PU foams, do not align anymore this chemistry with the EU's directives (REACH, Green Deal, Plastics Recycling Strategy)[5,6,7]. In this context, the efforts are now dedicated to developing alternative methods for producing safer PU foams that eliminate the use of isocyanates while ideally improving their environmental footprint.

Non-isocyanate polyurethanes (NIPUs) can be formed through a polyaddition reaction between a polyamine and a poly(cyclic carbonate), resulting in polyhydroxyurethanes[8-11]. The attractiveness of this process lies in the potential for both poly(cyclic carbonate)s and amines to be bio- and/or CO_2-derived[12]. For instance, poly(cyclic carbonate)s are prepared via CO_2 insertion into polyfunctional epoxides, which can be sourced from renewable resources like plant oils or sugars[13]. Similarly, some commercially available diamines, such as hexamethylene diamine (HMDA) and m-xylylene diamine (mXDA), isophorone diamine (IPDA), can be derived from bio-based precursors like starch, furfural. or renewable acetone, respectively[14-16]. However, a key challenge with polyhydroxyurethanes formation is the inherently low reactivity of amines

towards cyclic carbonates[17]. There have been numerous attempts to create NIPU foams (NIPUFs) using both external and internal blowing methods: External blowing approaches include the use of physical blowing agents such as solkane[18], supercritical carbon dioxide[19], acetone[20], or capitalize on the chemical decomposition of salts - e.g., inorganic carbonate salts with maleic acid – to generate the blowing agent[21,22]. Self-blowing attempts have also been made using hydrogen gas release[23-26], specific carbonate monomer-dependent decarboxylation[27], and the use of latent amine-carbon dioxide adducts[28]. However, these self-blowing methods often encounter limitations in industrial scalability due to safety concerns, extended reaction times, the need for external heat sources, or reliance on specific monomers for CO_2 production. These factors hinder the versatility and widespread adoption of these approaches[36].

In recent years, significant progress in creating CO_2 self-foaming NIPUFs has been reported by our group[29,30,35,36] and further exploited by others[31-34]. The foaming concept exploits a divergent cyclic carbonate ring opening strategy that involves competitive aminolysis and decarboxylative S-alkylation reactions (***Figure 1A***)[29-34]. While this approach successfully formed the NIPU network and induced foaming via CO_2 release, it still required an external heat source (120 °C) and a reaction time of 30 minutes, even after further development. In 2022, our group discovered that introducing water with a basic catalyst could induce foaming through cyclic carbonate hydrolysis while still achieving matrix cross-linking yet delivering a mimic of the foaming process of conventional PUs[35]. However, like the previous method, this approach also required external heat of 100 °C and a reaction time of 30 minutes (***Figure 1B***). In 2023, we achieved a fast foaming NIPUF from room temperature (RT) formulations by exploiting exothermic reactions in cascade (***Figure 1C***)[36]. By adding an epoxide as a heat release promotor within the NIPU formulation, a synergistic effect between aminolysis of both epoxide and cyclic carbonate moieties spontaneously increased the formulation temperature very rapidly, suppressing the need for external heating, yet resulting in a foam fabrication in about 5 minutes. However, the resulting material was a hybrid NIPU containing both hydroxyurethane and aminoalcohol linkages.

Herein, we resolve the challenge of producing 100% NIPU foams via an ultra-fast water-induced CO_2 self-foaming process initiated from RT formulations by utilizing an exo-vinylene cyclic carbonate (αCC) as an internal heat release promotor ***(Figure 1D)***. αCC displays significant reactivity against *N*-, *O*-, or *S*-nucleophiles[37,38,39]. Notably, their aminolysis by primary amines delivers hydroxyoxazolidones, i.e., a class of 5-membered cyclic urethanes. This reaction is extremely fast at RT even under catalyst-free conditions, and its highly exothermic nature becomes an asset in the creation of pure NIPU self-foaming materials when combined with cyclic carbonates/amines/water reactive formulation. Our methodology is first proven in concept by monitoring the exotherm of the reaction and by fabricating NIPUFs within minutes from RT formulations. Then, we deeply investigate the foaming mechanism, and we study the influence of the αCC microstructure on the foaming process and heat release, as well as on the thermo-mechanical foam's properties.

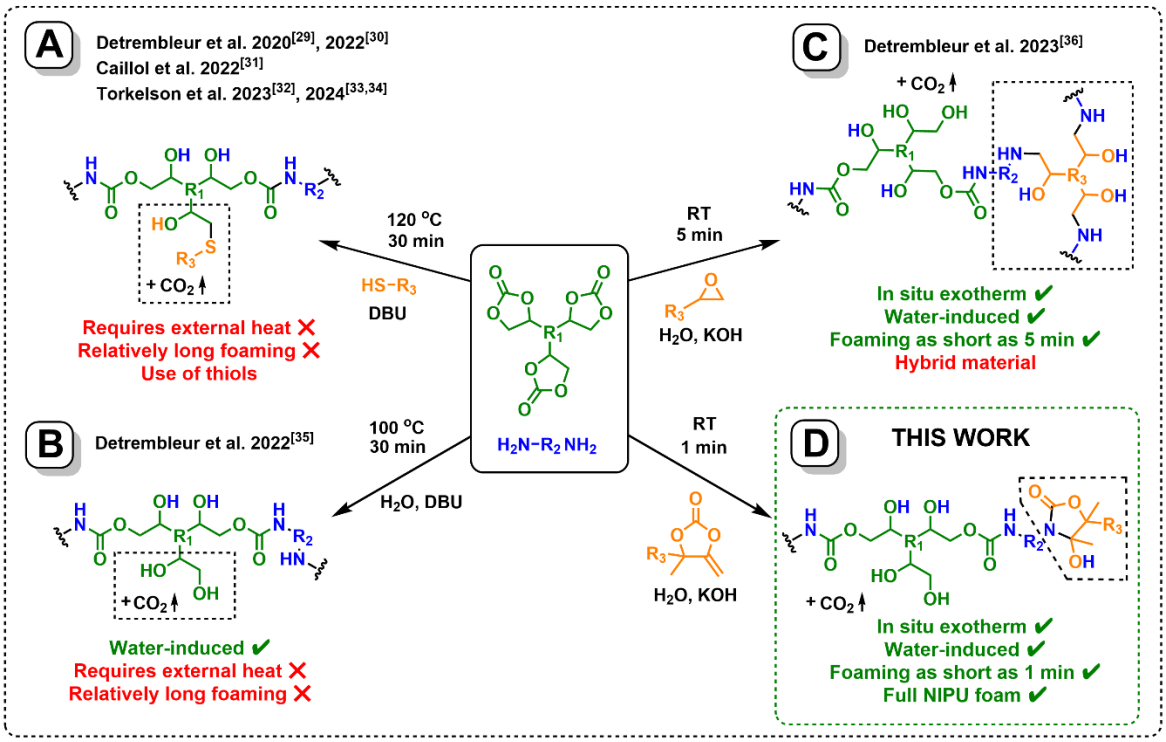

Figure 1. *A simplified scheme of CO_2 self-foaming technologies of NIPUFs (**A-C**) and the concept illustrated in this work (**D**): **A** – Self-blowing NIPUF via thiol-induced decarboxylation of cyclic carbonates; **B** – Water-induced CO_2 self-foaming of NIPUFs; **C** – Water-induced RT fast foaming of **hybrid NIPUFs** by exploiting exothermic reactions in cascade; **D** – CO_2 self-foaming of **100% NIPUFs** by water-induced RT fast foaming using exo-vinylene cyclic carbonates as heat release promotors.*

2. Results and Discussions.

2.1. αCC aminolysis exotherm and its impact on foaming.

Recently, we elaborated a cascade exotherm strategy to fabricate PHU foams from RT reactive poly(cyclic carbonate)/polyepoxide/polyamine/water formulations. This approach leverages the heat released in situ by running in a parallel fashion but at distinct rates for different reactions, i.e., the aminolysis of both the cyclic carbonates and the epoxides (for the polymer matrix construction) and the hydrolysis of 5CC (furnishing the blowing agent). Despite being very efficient, this methodology delivers foams of hybrid epoxy-urethane microstructure. Thus, we capitalize on the unique reactivity of alkylidene cyclic carbonates (αCC) with *N*-nucleophiles to generate sufficient heat in situ and impulse the formation of pure NIPU foams within minutes from RT formulations. To validate our strategy, the exothermicity of the amine/αCC reaction is first highlighted by using a model αCC (4,4-Dimethyl-5-methylene-1,3-dioxolan-2-one, DMACC) and 1-heptylamine under solvent-free conditions. An expedited temperature rise from 25 °C to 160 °C was observed in less than 1 minute ***(Figure S1).*** Then, DMACC has been added to a standard NIPU foam formulation containing a tri(cyclic carbonate) (TMPTC), a triamine (TREN), water (the chemical blowing agent), the catalyst (KOH), and hydrotalcite (HTC) as a filler ***(see Table 1, and S2-3 in ESI for all formulations)***. Formulations ***F1***, ***F3,*** and ***F5*** were also prepared with an epoxide (TMPTE), substituting DMACC, solely for comparison of generated exotherms ***(Figure 2A)***. The exotherm was sufficient to induce the ultrafast foam expansion within 30 seconds, and the foaming zone of ~ 100 °C already reached with 0.1 eq. αCC *vs.* 5CC (***Figure 2B***). Also, as can be seen in ***Figure 2B***, the possibility to control the exotherm of the foaming process was also present. By varying the αCC *vs.* 5CC content from 0.1 eq. up to 0.3 eq., the maximum temperature of the reactive formulation increased from 110 °C to 130 °C. Importantly, the exotherm appeared more rapidly with αCC than with the epoxide (***Figure 2B***).

***Table 1**. NIPUF formulations expressed in mol eq. to 5CC; **a -** Same formulation applied with αCC substituted with TMPTE. **b -** The filler was used with a 10 wt% to poly(cyclic carbonate).*

Formulation	Components with their eq. to 5CC in the formulation						
	TMPTC (5CC)	**Amine 1 (NH_2)**	**Amine 2 (NH_2)**	**αCC**	**H_2O**	**Cat.**	**Filler[b]**
F1	TMPTC 1	TREN 0.95	-	DMACC 0.10 [a]	0.15	KOH 0.075	HTC
F2	TMPTC 1	TREN 1.00	-	DMACC 0.15	0.15	KOH 0.075	HTC
F3	TMPTC 1	TREN 1.05	-	DMACC 0.20 [a]	0.15	KOH 0.075	HTC
F4	TMPTC 1	TREN 1.10	-	DMACC 0.25	0.15	KOH 0.075	HTC
F5	TMPTC 1	TREN 1.15	-	DMACC 0.30 [a]	0.15	KOH 0.075	HTC
F6	TMPTC 1	TREN 1.15	-	DMACC 0.25	0.10	KOH 0.05	HTC
F7	TMPTC 1	TREN 1.05	-	DMACC 0.25	0.20	KOH 0.1	HTC
F8	TMPTC 1	TREN 0.81	mXDA 0.35	DMACC 0.25	0.10	KOH 0.05	HTC
F9	TMPTC 1	TREN 0.81	HMDA 0.35	DMACC 0.25	0.10	KOH 0.05	HTC
F10	TMPTC 1	TREN 0.81	EDR-148 0.35	DMACC 0.25	0.10	KOH 0.05	HTC

F11	TMPTC 1	TREN 0.81	IPDA 0.35	DMACC 0.25	0.10	KOH 0.05	HTC
F12	TMPTC 1	TREN 1.05	-	*i*-BuMACC 0.25	0.10	KOH 0.05	HTC
F13	TMPTC 1	TREN 1.05	-	CHACC 0.25	0.10	KOH 0.05	HTC
F14	TMPTC 1	TREN 1.05	-	MPACC 0.25	0.10	KOH 0.05	HTC

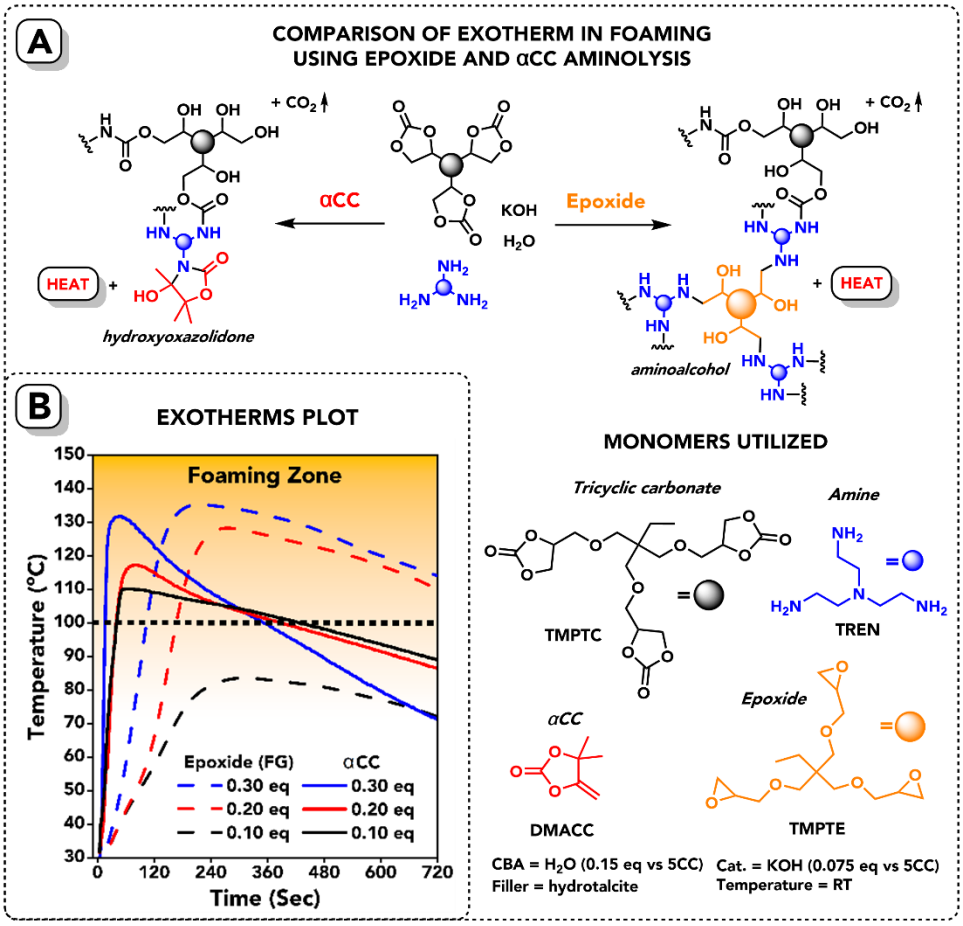

***Figure 2**. A simplified scheme focusing on aminolysis reactions in PHU foaming formulations with resulting heat generation profiles. **A** - Aminolysis of DMACC and TMPTE monomers utilized in foaming formulations, along with foaming formulation equivalents; **B** – plot of recorded temperature vs. time, showcasing the exotherm during foaming with formulations **F1**, **F3**, **F5** using either αCC or epoxide as a heat release promotor. The equivalents of **0.1**, **0.2**, and **0.3** are molar ratios of αCC or epoxide groups to 5CC groups, (see **Table 1**, and **S2-3** in ESI for all formulations; section 6.3.3. for NIPUF synthesis conditions).*

The production of foams for different contents of αCC is illustrated in ***Figure 3***, highlighting the significant impact of αCC content on foam porosity. Changing the αCC content influenced the foam porosity, with larger cells being formed at higher αCC content due to their lower stabilization. Complementing this visual data, ***Figure 4A*** provides the

quantitative evaluation in terms of total density and inner average density of the obtained opened cell foams, as well as their gel content. As the content of αCC decreased from 0.30 eq. to 0.15 eq., the total density of the foams increased from 173 kg m^{-3} to 323 kg m^{-3}, and the inner average density rose from 58 ± 15 kg m^{-3} to 152 ± 12 kg m^{-3}(***the results are summarized in table S4 in ESI***). For the lowest αCC content (0.1 eq. αCC), no foaming was observed. The disparity between overall density and inner density is attributed primarily to creaming, where gas bubbles migrate toward the foam surface due to low viscosity and insufficient bubble stabilization. This phenomenon is particularly noticeable at the foam's base and may also be influenced by spatial limitations during foam expansion and differing heat transfer rates along the HDPE cup surface, which affect reaction rates at the inner surface.

As DMACC is a monofunctional molecule, it terminates NIPU chains, yet it affects the cross-linking density of the material. The gel content of the foams increased from 89% at a high αCC content (0.3 eq. *vs.* 5CC) to 97% with 0.15 eq. of αCC. Additionally, the glass transition of foams equilibrated at 30% humidity at RT ($T_{g,\ eq.}$) was also dependent on the αCC content (***Figure 4B***). $T_{g,\ eq.}$ values ranged from 28 to 36 °C, increasing with decreasing αCC content, which indicated a decreased hydroplasticization. However, the glass transition measured on dried samples ($T_{g,\ dry}$) was only slightly affected by the αCC content (ranging from 46 to 47.5 °C) (***see Figures S2-5 of ESI for full DSC thermograms***). As shown in ***Figure 4C***, foams ***F2-5*** displayed rather similar degradation behaviors (***see figures S6-9 of ESI for full TGA thermograms***). The $T_{d,\ onset}$ was measured at 198 ± 2 °C, as a prior mass loss that is related to dehydration of hydroxyoxazolidone moieties[41,42], and the $T_{d,\ 5\%}$ was at 248 °C. These values align with the typical degradation range of commercial PUFs, which is between 230-300 °C[43,44], and to PHU foams prepared by the water-based system (250 °C)[34]. These results showed that the presence of oxazolidone moieties within the NIPU network did not significantly influence the thermal properties of the foams under their dried state (within the investigated range) but influenced the hydroplasticization of the foam by changing the water absorption.

FT-IR analyses were also conducted to elucidate the chemical structure of the foams (***Figure 4D***) with a main focus on two key elongations: the carbonyl band of 5CC at 1790 cm^{-1} and the urethane carbonyl band at 1695 cm^{-1}(***see figure S10 in ESI for full, stacked FT-IR spectra).*** Qualitatively, an increase of the αCC content led to a higher proportion of unreacted 5CC groups within the foam. Also, identifying the characteristic C=O stretch of formed hydroxyoxazolidone (at 1660 cm^{-1}) was challenging due to its overlap with the C=O stretch of urethane (at 1695 cm^{-1}). This overlap, combined with the low content of αCC in the formulation, makes it difficult to conclusively isolate the hydroxyoxazolidone signal using this method. Based on these results, it was determined that using 0.25 eq. of αCC vs. 5CC (foam ***F4***) provided the adequate exotherm for this foaming system, yielding NIPUFs with a nearly complete conversion of 5CC groups.

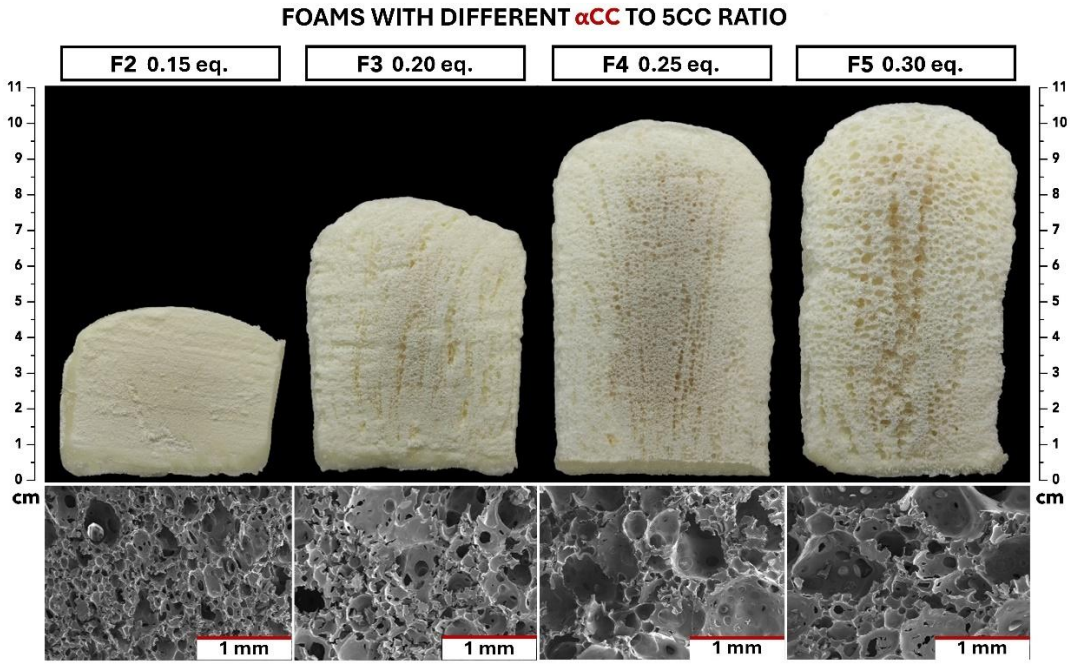

Figure 3. *The cross-section images of NIPUF formulations* ***F2-5****, made with different DMACC (αCC) equivalents to 5CC, and x50 zoom SEM images of inner foam (see* ***Table 1****, and* ***S2-3*** *in ESI for all formulations; section 6.3.3. for NIPUF synthesis conditions).*

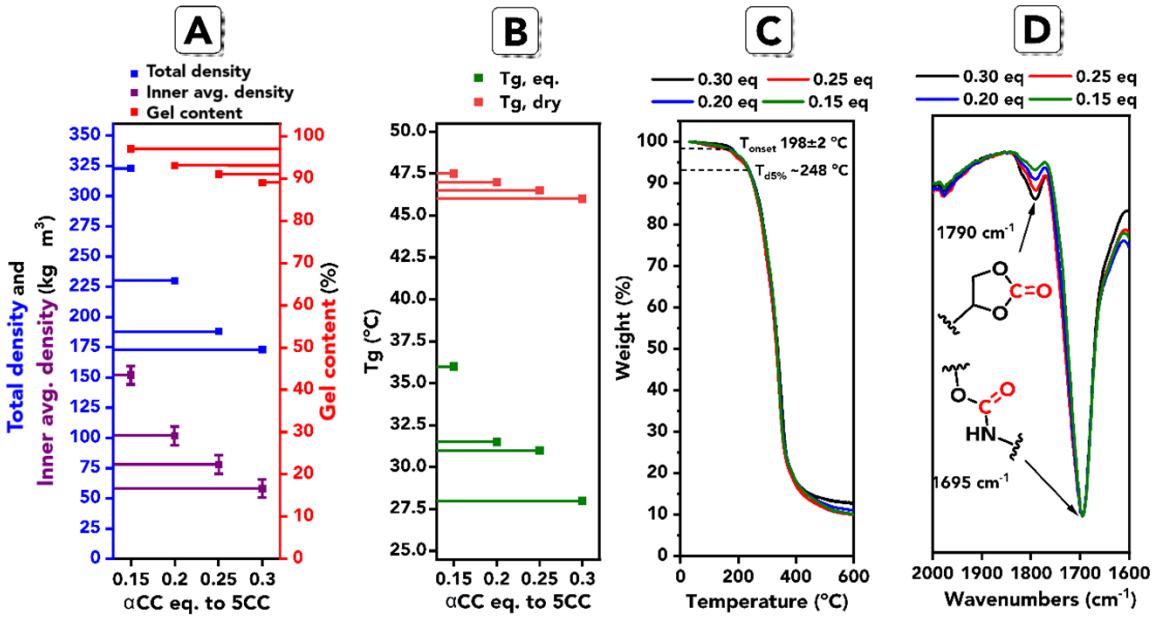

Figure 4. *Characteristics of* ***F2-5*** *PHUFs across varying DMACC (αCC) contents within the formulation.* ***A*** *– Left Y axis: Density values vs. DMACC to 5CC content in the formulation (Total Density blue-colored lines, Inner average Density purple-colored lines). Right Y axis: Gel Content (red lines) vs. DMACC to 5CC content in the formulation;* ***B*** *– Plot of both equilibrated and dry T_g vs. DMACC eq. to 5CC, estimated by DSC.* ***C*** *– superimposed weight loss vs. temperature plot of PHUFs* ***F2-F5*** *obtained by TGA;* ***D*** *- Superimposed FT-IR spectra, normalized on 1695 cm^{-1}carbonyl stretch.*

Building on ***F4*** (foam with 0.25 αCC eq. to 5CC), we investigated the impact of varying the water content on the foam characteristics. Specifically, we adjusted the water molar eq. to 5CC, to two different values: 0.10 eq. (foam ***F6***) and 0.20 eq. (foam ***F7***), while 0.15 eq. was present in ***F4***. As expected, the water amount was crucial for optimizing the morphological characteristics on such PHUFs (***Figure 5***). The lowest water content (0.10 eq.) delivered a NIPU foam with a more homogeneous morphology by limiting excessive hydrolysis of 5CC groups, which in turn promoted better cross-linking and stabilization of the material. In contrast, higher water eq. (0.20 eq.) led to inhomogeneous foam structures, with some collapse attributed to increased hydrolysis and reduced cross-linking, which hindered foam stability.

A higher water content increased 5CC hydrolysis, resulting in a reduced degree of cross-linking in the polymer matrix, as was indicated by the lower gel content in ***F7*** (89%) compared to ***F6*** (98%) with a lower water content (***Figure 6A***). Consequently, the total foam density decreased from 233 kg m^{-3} to 168 kg m^{-3}, while the inner average density dropped from 128 ± 15 kg m^{-3} to 65 ± 15 kg m^{-3} as the water-to-5CC ratio increased from 0.10 to 0.20 eq. (***the results summarized in table S5 in ESI***). This trade-off between foam expansion and cross-linking highlights the delicate balance required to optimize foam properties.

The DSC analysis (***Figure 6B***) revealed that $T_{g,\,eq.}$ dropped from 31 °C in formulation ***F4*** to 26 °C in formulation ***F7***, while formulation ***F6*** had a very similar $T_{g,\,eq.}$ to ***F4*** (***see Figures S11-12 of ESI for full DSC thermograms***). However, $T_{g,\,dry}$ of these foams showed only minor variations, indicating that the differences in room-equilibrated samples were due to hydroplasticization. This was confirmed by TGA analysis results (***see Figure 6C***), where the $T_{d,\,onset}$ for formulation ***F7*** was estimated at 130 °C due to mass loss from water evaporation (***see figures S13-14 of ESI for full TGA thermograms***). FTIR studies confirmed the nearly complete conversion of 5CC in formulation **F6**, as shown by the near-total disappearance of the 5CC carbonyl elongation at 1790 cm^{-1} (***Figure 6D***) (***see figure S15 in ESI for full, stacked FT-IR spectra).***

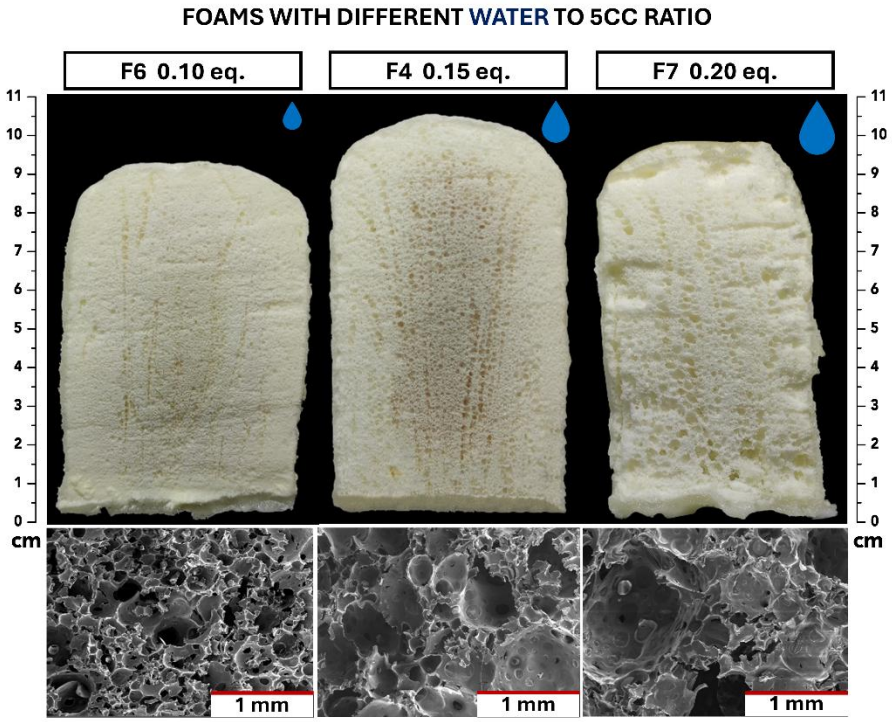

Figure 5. *The cross-section cut images of NIPUF formulations* ***F4*** *and* ***F6-7****, made with different water equivalents to 5CC, and x50 zoom SEM images of inner foam (see Table 1, and S2-3 in ESI for all formulations; section 6.3.3. for NIPUF synthesis conditions).*

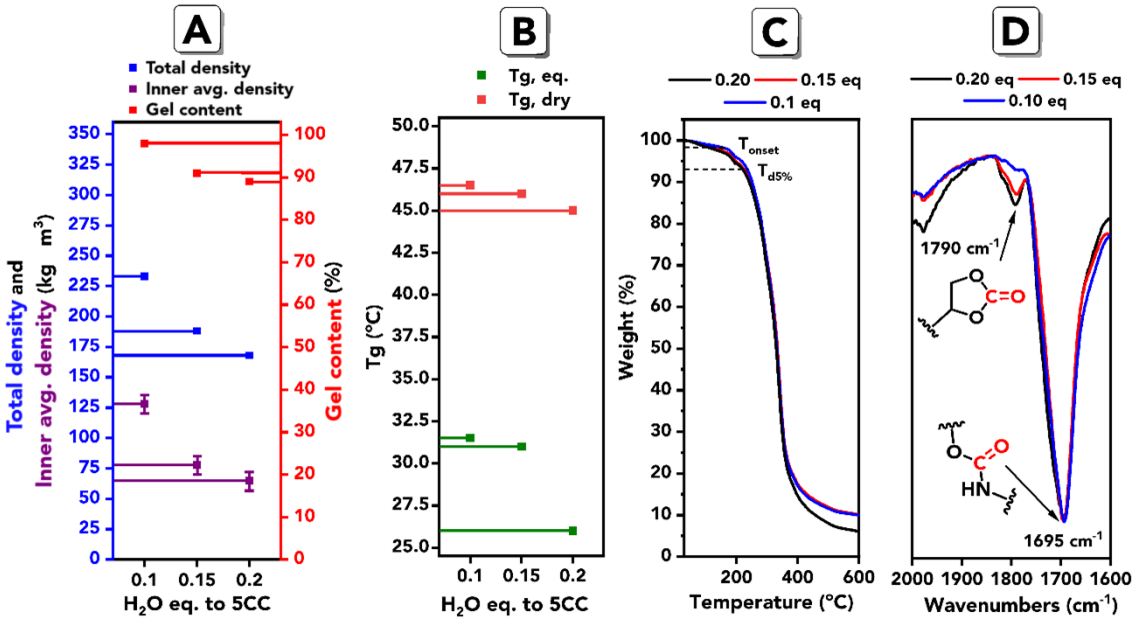

Figure 6. ***F4***, ***F6-7*** *NIPUFs characteristics vary H_2O to 5CC eq. within the formulation.* ***A*** *– Left Y-axis: Density values vs. water to 5CC eq. in the formulation (Total foam density blue-colored lines, inner average density purple-colored lines). Right Y-axis: Gel content (red lines) vs. water to 5CC eq. in the formulation.* ***B*** *– Plot of both equilibrated and dry T_g vs. H_2O eq. to 5CC, estimated by DSC;* ***C*** *– Superimposed weight loss vs. temperature plot of NUPUFs* ***F4***, ***F6-7***, *obtained by TGA;* ***D-*** *Superimposed FT-IR spectra, normalized on 1695 cm^{-1}carbonyl stretch.*

2.2. Foaming mechanism.

The two cyclic carbonate groups involved in the foaming process, αCC and 5CC, are both prone to hydrolysis and aminolysis. While the partial hydrolysis of 5CC is needed to generate the blowing agent (CO_2), the one of αCC should be avoided as it will, besides the formation of CO_2, produce the corresponding hydroxyketone that would not be incorporated into the PHU network and consequently would contaminate the foam. The rates of aminolysis and hydrolysis of these two cyclic carbonates have thus to be determined to elucidate the chemical structure of the foam. As the foams are thermosets,

the characterization tool set is very limited. We therefore carried out model reactions on monofunctional molecules to permit the characterizations by ^{1}H-NMR spectroscopy. For that purpose, we studied the aminolysis of DMACC (the model αCC) and propylene carbonate (PrC; the model 5CC) by 1-heptylamine and compared their rates with those of their hydrolysis. ***Figure 7A*** shows the expected products, and ***Figure 7B*** depicts the rate of consumption of the different reagents and the yields in the different products determined by ^{1}H-NMR analysis (***see ESI sections 3.4.1, 3.4.2 for experimental protocols***).

For this study, similar contents in the functional groups than in the foaming formulation ***F6*** were used: 1 eq. PrC (5CC), 0.25 eq. DMACC (αCC), 1.15 eq. 1-heptylamine, 0.1 eq. water, and 0.05 eq. KOH. The reaction was also carried out without any solvent at room temperature. Immediately after mixing, a rapid exotherm was recorded, reaching 95 °C, which was 30 °C lower than in the foaming case (orange line in ***Figure 7B***). Due to the low viscosity of the model reaction mixture, the generated heat dissipated quickly, enhancing heat transfer. Nevertheless, results indicated that DMACC was rapidly consumed by aminolysis, reaching 100% consumption after 30 seconds with the selective and quantitative formation of the corresponding hydroxyoxazolidone. Neither the oxo-urethane intermediate for DMACC aminolysis[38], suggesting immediate cyclization into hydroxyoxazolidone, nor the dehydration of oxazolidone were detected, indicating these adducts have a low occurrence during foaming. Importantly, the aminolysis of DMACC was faster than its hydrolysis, as the hydroxyketone adduct was not visible (yield below 0.1%) (***Figure 7B right)***. It's worth noting that the low hydrolysis rate was also driven by the difference in stoichiometry between amine and water (***see Figure S16 for ^{1}H-NMR***).

The consumption of PrC has occurred more slowly, with only 25% consumption after 1 minute (compared to 100% for DMACC) (***Figure 7B right***). Unlike DMACC, both the hydrolysis and aminolysis of PrC were observed with a quite similar rate, leading to the hydroxyurethane and propanediol products. Note that the lower exotherm generated by the model compounds hindered the full consumption of PrC by both aminolysis and hydrolysis (50-60% yield), in contrast to the foaming process since both reactions are highly influenced by temperature[41].

Then, to study the rates of both aminolysis and hydrolysis of αCC, the experiment was carried out under stoichiometric conditions (αCC: amine: H_2O: KOH = 1:0.5:0.5:0.25) excluding PrC (***see Figure S17***). As in the previous assay, after mixing, a rapid exotherm was also recorded, reaching 130 °C, which is nearly in the same exotherm range as during foaming (***see Figure S18***). The aminolysis and hydrolysis yields were more balanced (80:20), though still favoring aminolysis (***see Figure S19 for ^{1}H-NMR spectra)***. To confirm that the hydrolysis of DMACC did not occur during foaming, we produced NIPU foam ***F6,*** and no hydroxyketone was extracted by dipping the foam in THF for 72 h (***see Figure S20 for ^{1}H-NMR spectra and S21 for ^{13}C-NMR spectra***).

These studies suggest that 5CC was the primary source of the blowing agent through hydrolysis, while DMACC underwent rapid aminolysis to form hydroxyoxazolidone at the early stages of the foaming process. The resulting PHUFs mainly contain hydroxyurethane linkages, vicinal diol, and hydroxyoxazolidone pendant groups.

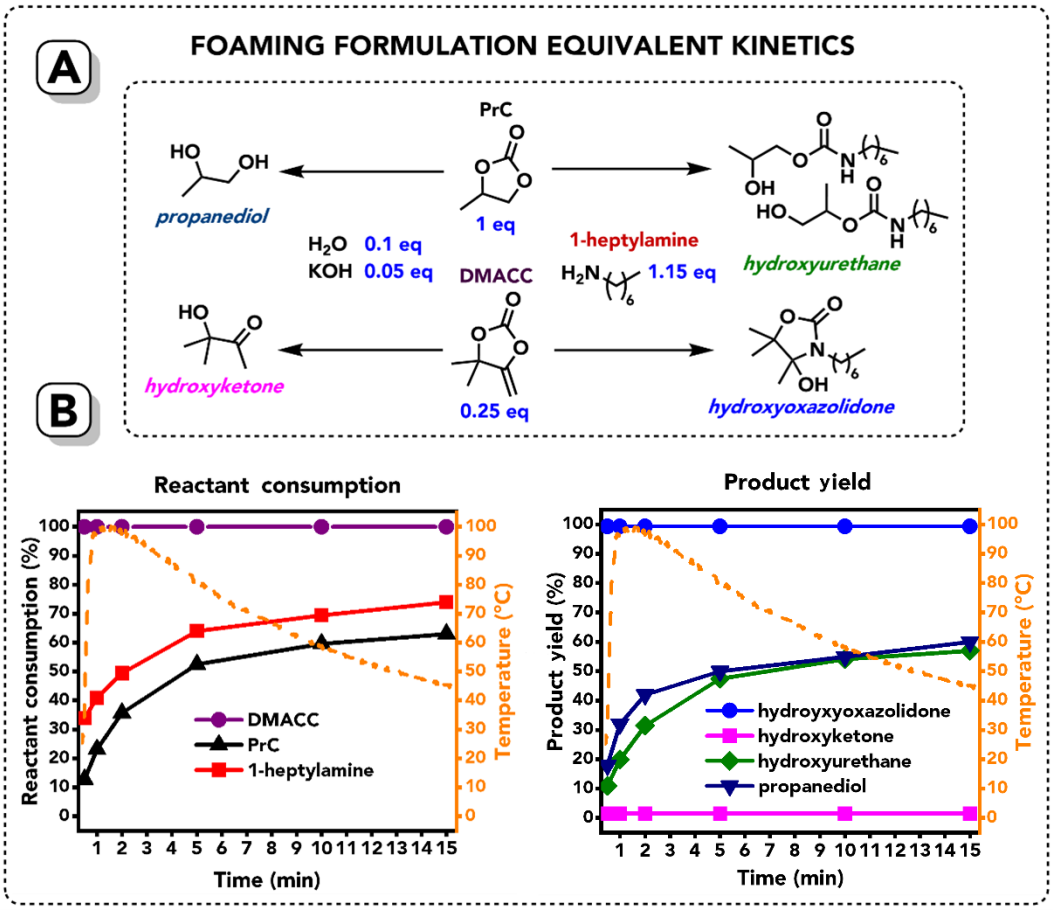

Figure 7. *Model reactions mimicking foaming with formulation* ***F6****.* ***A*** *– depicts the in situ reactions that potentially occur during foaming, with reactant equivalents simulating monomer equivalents in formulation* ***F6****;* ***B*** *– consists of two plots. The* ***left*** *plot shows the consumption of DMACC, PrC, and 1-heptylamine over time. The* ***right*** *plot illustrates the yields of hydrolysis (propanediol, hydroxyketone) and aminolysis products (hydroxyurethane, hydroxyoxazolidone) over time. In both plots, the orange dashed line represents temperature vs. time, sharing the Y-axis (temperature) with reactant consumption and product yield.*

2.3. Versatility of technology.

The success story of PUFs is directly linked to the ability to modulate their mechanical properties by adjusting the formulation composition, such as changing the nature of the polyol or isocyanate. Similarly, recent work has demonstrated that the properties of PHUFs are significantly influenced by the choice of the amine, cyclic carbonate, and the epoxide[36]. Herein, we evaluated the influence of the nature of the αCC on the foamability and the properties of the resulting foams. For this purpose, DMACC was replaced by αCCs bearing an aromatic (MPACC), cycloaliphatic (CHACC), or a branched aliphatic (iBuMACC) substituent in the foam formulation ***F6*** (***Figure 8A***).

The nature of the αCCs noticeably influenced the exotherm profile during foaming, as shown in ***Figure 8B***. Specifically, the formulation with CHACC (***F13***) behaved similarly to the formulation with DMACC (***F6***) in terms of maximum temperature and further heat dissipation. However, visual observations of the reactive mixtures with MPACC (***F14***) and iBuMACC (***F12***) suggested a thicker, more viscous consistency. Interestingly, the foam expansion time of formulations ***F12-14*** was slightly delayed from 30 seconds to approx. 1.5 minutes, presumably due to introduced steric hindrance on new monomers, however, the exotherm was emitted rapidly as in previous cases. We believe that the observed higher viscosity was related to a faster gelation time, plus correlated with a slower heat dissipation and a more prolonged heat release, keeping the temperature within the foaming zone longer (dashed line in ***Figure 8B***). These visual observations suggested that the increased viscosity extended the curing time while maintaining a high exotherm. Despite this, FT-IR analysis of the inner part of the resulting foams indicated similar conversions of 5CC in all cases (***Figure 8C; see Figures S22-24 for full FT-IR spectra***).

As can be seen in ***Figure 9***, the slightly delayed foam expansion impacted the cell structure of the foam, preserving the open-cell structure but much more defined and homogeneously distributed. Speaking of cell size change from DMACC formulations, it is complicated to estimate the average cell size since rapid expansion is strongly damaging cells. However, on formulations ***F12-14***, the cells are much more well defined but smaller in size, thus the zoom of x100 was applied instead of x50 as in previous cases. Examining

the cell sizes, it can be observed that formulation ***F6*** exhibited pores with an average size of 157 ± 20 µm, while formulations ***F12–14*** displayed sizes ranging from 85 ± 15 µm (***F12***) to 180 ± 45 µm (***F13***), with ***F14*** having an intermediate size of 133 ± 30 µm. These values fall within the typical range for semi-rigid PU foams (100–200 µm) [4].

Fillers also play a key role in cell size, with their shape, size, and exfoliation extent significantly affecting cell count and dimensions [29,36]. Hydrotalcite, in particular, enhances homogeneity by stabilizing viscosity and acting as a foam nucleating agent [35-36], and prevents combustion through its endothermic decomposition[45]. The necessity of incorporating a filler was further substantiated by repeating the ***F6*** formulation without hydrotalcite, where the resulting foam structure was highly unstable and failed to form a coherent foam despite visible gas release (***Figure S25 of the ESI***). Note that a 10 wt% HTC *vs.* TMPTC was used in this study, which revealed to be in the range of appropriate contents for providing homogeneous NIPU foams by our water-induced foaming processes [35-36].

The characteristics of the PHUFs produced with different αCCs are summarized in ***Table 2***. The foam made with iBuMACC (***F14***) showed the lowest expansion, with a total density of 390 kg m^{-3} and an inner density of 231 ± 5 kg m^{-3}, suggesting that the branched aliphatic structure of iBuMACC increased viscosity and slowed gas release during foaming. Other formulations with CHACC (***F15***) and MPACC (***F16***) produced foams with similar total densities (~270 kg m^{-3}) and lower inner densities (173 ± 7 kg m^{-3}), indicating the potential for better foam expansion.

Gel content was consistently high across all samples, ranging from 91% (iBuMACC) to 98% (MPACC, DMACC), reflecting effective cross-linking. The slightly lower gel content of iBuMACC-based foams (GC = 91%) suggests reduced cross-linking efficiency, likely tied to the branched structure slowing gelation. This variation in cross-linking could influence mechanical properties, with MPACC providing a more tightly linked polymer network. The $T_{g,\,eq.}$ varied between 28 and 37.7 °C for the $T_{g,\,eq.}$, while formulations with CHACC and MPACC exhibited higher $T_{g,\,eq.}$ values. Similarly, the $T_{g,\,dry}$ followed this trend, with CHACC-based foams showing the highest T_g, dry at 60.3 °C, highlighting the

influence of the cycloaliphatic structure in improving thermal performance (***see Figures S26-28 for full DSC thermograms***). However, thermal stability, reflected by $T_{d,\ 5\%}$, remained relatively close across all samples, ranging from 225 °C to 240 °C, indicating comparable resistance to thermal degradation despite variations in gel content and T_g values (***see Figures S29-31 for full TGA thermograms***).

These results suggested that while the content of αCC was quite low (0.25 eq. *vs.* 5CC), the choice of αCC influenced cross-linking and T_g, and the overall thermal degradation characteristics of the foams were similar. Interestingly, the choice of αCC dictated the foam density, allowing for adjustment of the formulation for a targeted application.

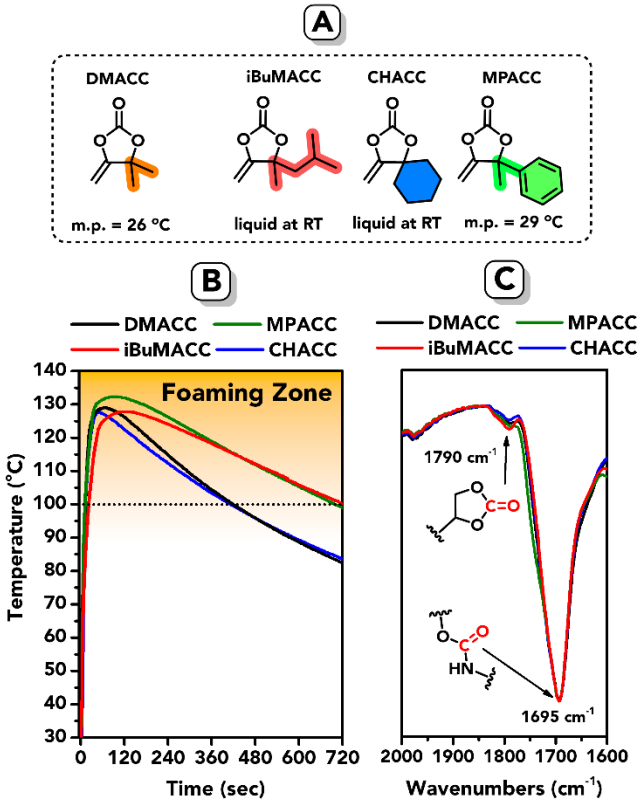

***Figure 8**. Effect of αCCs with different substituents on the foaming exotherm and 5CC conversion. **A** – αCCs monomers used in the assay; **B** – Superimposed plots of temperature vs. time, showcasing recorded exotherms during foaming with formulations **F6**, **F12-14**; **C –** Superimposed normalized FT-IR spectra of grinded foams **F6**, **F12-14**, (see **Table 1**, and **S2-3** in ESI for all formulations; section 6.3.3. for NIPUF synthesis conditions).*

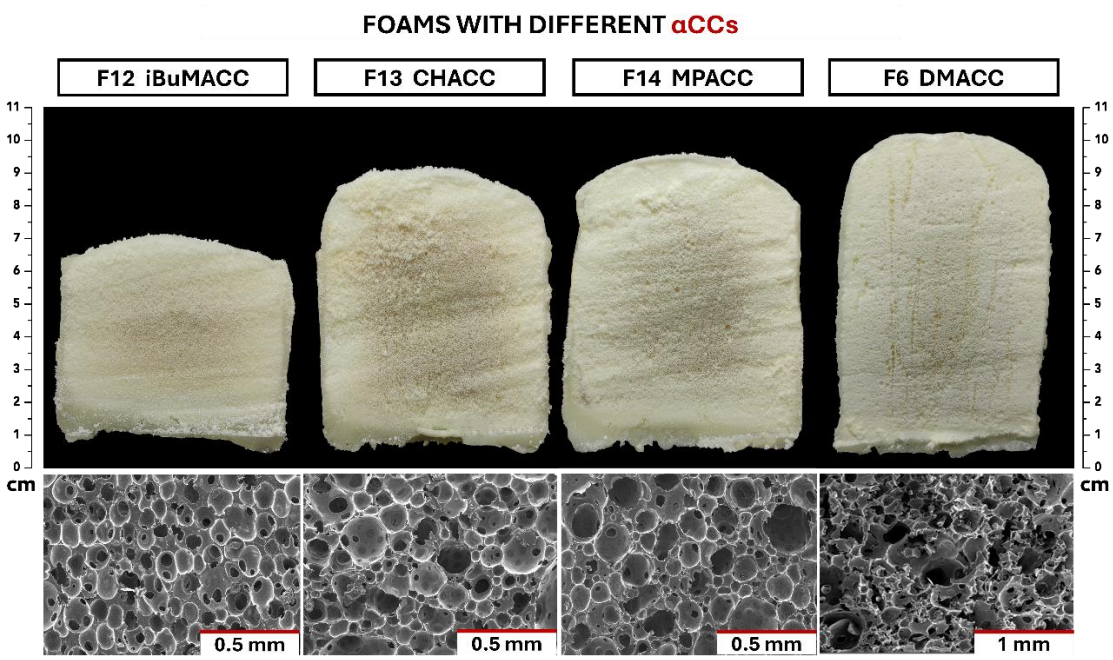

***Figure 9.** The cross-section images of NIPUF formulations **F6** (reference) and **F12-14**, made with different αCCs, and SEM images (x50 zoom for **F6**; x100 zoom for **F12-14**) of inner foam, (see **Table 1**, and **S2-3** in ESI for all formulations; section 6.3.3. for NIPUF synthesis conditions).*

Table 2. *Characterization of PHUFs produced by utilizing different αCCs, (see* ***Table 1*** *and* ***S2-3*** *in ESI for all formulations; section 6.3.3. for NIPUF synthesis conditions). * Properties of* ***F6*** *used as a reference.*

Entry	αCC	Total density, (kg × m^{-3})	Inner average density, (kg × m^{-3})	Gel content, (%)	$T_{g,\ eq.}$, (C°)	$T_{g,\ dry}$, (C°)	$T_{d,\ 5\%}$, (C°)
F6*	DMACC	233	128 ± 15	98	31.5	46.5	244
F12	^{i}BuMACC	390	231 ± 5	91	32.5	45.9	240
F13	CHACC	272	166 ± 7	96	37.7	60.3	240
F14	MPACC	271	180 ± 11	98	28	56.7	236

In a similar way, the nature of the amine was investigated by replacing TREN with more flexible (EDR 148, 2,2'-(ethane-1,2-diylbis(oxy))bis(ethan-1-amine) or HMDA, hexamethylenediamine) or less flexible amines (mXDA, meta-xylylenediamine, or IPDI, isophoronediamine) (***Figure 10A,B***).

However, we discovered that if the triamine content in the amine mixture was lower than 70 mol%, the foam shrank during cooling. This behavior was likely due to a mismatch between the gelation and expansion rates, caused by the lack of stabilization of the expanded matrix. Indeed, we observed that the gel content of the foams dropped from 98% when the formulation contained TREN only to 85-89% with 30 mol% of diamine, confirming the lower cross-linking degree of the foams containing the mixture of diamine and triamine.

According to FT-IR analysis, formulations ***F8***, ***F9,*** and ***F11*** undergo nearly absolute conversion of 5CC groups, while in formulation ***F10***, some unreacted 5CC groups were present (***Figures S32-35***). When using 30% of difunctional mXDA (***F8***) or IPDA (***F11***) as diamine, the gel content of the foam dropped from 98% to 85% or 89%, respectively, and the room T_g decreased from 31.5 °C to 29 °C, while the dry T_g increased from 46.5 °C to 54 °C and 53 °C, indicating a significant improvement of thermo-mechanical properties under the dried state (***Figures S36-39***). In contrast, using 30% linear aliphatic amine HMDA (***F9***) or EDR-148 (***F10***) led to reductions in both T_g and gel content. The TGA analysis showed that formulations ***F8*** and ***F11*** both have a $T_{d,\,5\%}$ around 245±1 °C, while differing by 10 °C (200 °C for ***F8*** and 190 °C for ***F11***), and formulations ***F9-10*** showed $T_{d,\,5\%}$ 192 ± 1 °C formulations ***F9-11*** provided a close $T_{d,\,onset}$ value of 191±2 °C, while for $T_{d,\,5\%}$ ***F9*** showed 234 ºC, and ***F10*** showed 240 ºC (***Figures S40-43***; ***see Table 3 for a comparison of NIPUF properties***).

It is important to note that the exotherm was also lower when increasing the content of diamine in the formulation. For instance, by raising the mXDA content from 0 to 30 and 50%, the maximum temperature at the core of the foam was decreasing from 125 °C, to 115 °C and 108 °C, respectively (***Figure S44***). This lower exotherm also contributed to a slower cross-linking, consequently leading to some foam collapse.

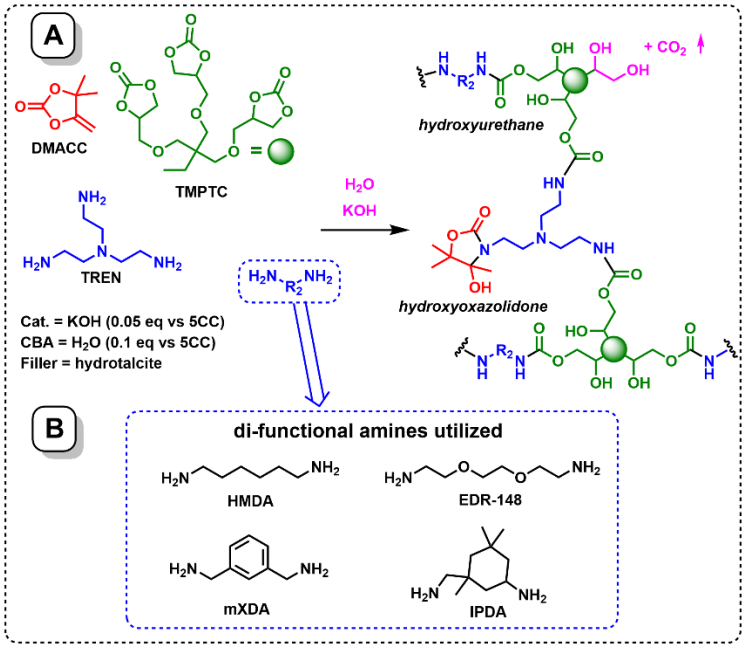

***Figure 10. A** – A scheme of foaming reactions in which a trifunctional amine, TREN, was introduced along with a varied diamine. **B** – monomers varied within foaming formulations **F8-F13**, (see **Table 1**, and **S2-3** in ESI for all formulations; section 6.3.3. for NIPUF synthesis conditions).*

Table 3. *Characterization of foams made with formulations* ***F6*** *(****reference****) and* ***F8-1****, utilizing different amines (see* ***Table 1****, and* ***S2-3*** *in ESI for all formulations; section 6.3.3. for NIPUF synthesis conditions). * Properties of* ***F6*** *used as a reference.*

Entry	5CC	Amine	Total density, (kg × m^{-3})	Inner average density, (kg × m^{-3})	Gel content, (%)	$T_{g,\ eq.}$, (C°)	$T_{g,\ dry}$, (C°)	$T_{d,\ 5\%}$, (C°)
F6*	TMPTC	TREN	233	128 ± 15	98	31.5	46.5	244
F8	TMPTC	mXDA/ TREN	238	110 ± 14	85	29	54	245
F9	TMPTC	HMDA/ TREN	243	116 ± 15	87	-4	44	234
F10	TMPTC	EDR-148/ TREN	280	179 ± 15	86	12	34	240
F11	TMPTC	IPDA/ TREN	304	143 ± 13	89	34	53	246

To achieve a comprehensive understanding of the nature of the diamine on the foam properties, three formulations were considered, each with a distinct composition: ***F6*** (reference), employing only TREN as the amine, ***F9*** with 70% TREN and 30% HMDA for expected flexible foam properties, and ***F8*** with 70% TREN and 30% mXDA for expected rigid foam properties. Importantly, since foam properties are influenced by ambient conditions and are prone to hydroplasticization, the three foams were equilibrated at different humidity percentages before testing under quasi-static compression. Results were compared to samples that were dried prior to analysis. It must be noted that the three foams have similar foam densities, which enabled a fair comparison of their mechanical properties. The compression tests, performed under a constant compression rate,

revealed distinct mechanical responses based on formulation and environmental conditions (***Figure 11A***).

Each foam exhibited characteristic stress-strain behavior, where the curve can be divided into three regions. Initially, the curve showed an elastic region where stress increased proportionally with strain, followed by a plateau region where cell collapse, or failure, was progressively observed. The final densification region occurred as the foam's cells were progressively compressed, leading to a sharp increase in stress with increasing strain. The Young's modulus was calculated from the linear elastic region of the curve (***see Table S6 for full data***). The dried formulations ***F6*** and ***F8*** displayed a rigid profile, with comparable Young's modulus values of 8.54 MPa and 9.0 MPa, respectively, while formulation ***F9*** showed flexible behavior with Young's modulus of 0.3 MPa. Increasing humidity induced plasticization, leading to significant softening of the materials. At 40% humidity, ***F6*** nearly lost its rigidity (modulus = 1.66 MPa), ***F8*** foam retained its rigid profile (modulus = 8.90 MPa), and ***F9*** turned highly flexible (modulus = 0.02 MPa). With further increases to 60% and 80% humidity, the trend persisted, eventually transforming all the foams into flexible ones with a modulus < 0.04 MPa. This was represented in ***Figure 11B***. These findings highlight the importance of the hydrophilic nature of NIPUFs on their mechanical properties with a decrease of the Young's modulus when exposed to increased humidity contents as the result of hydroplasticization. Adapting the foam composition also enabled them to easily tune their mechanical properties over a broad range of Young's modulus. This study underscores the importance of considering environmental factors when optimizing foam formulations for specific applications.

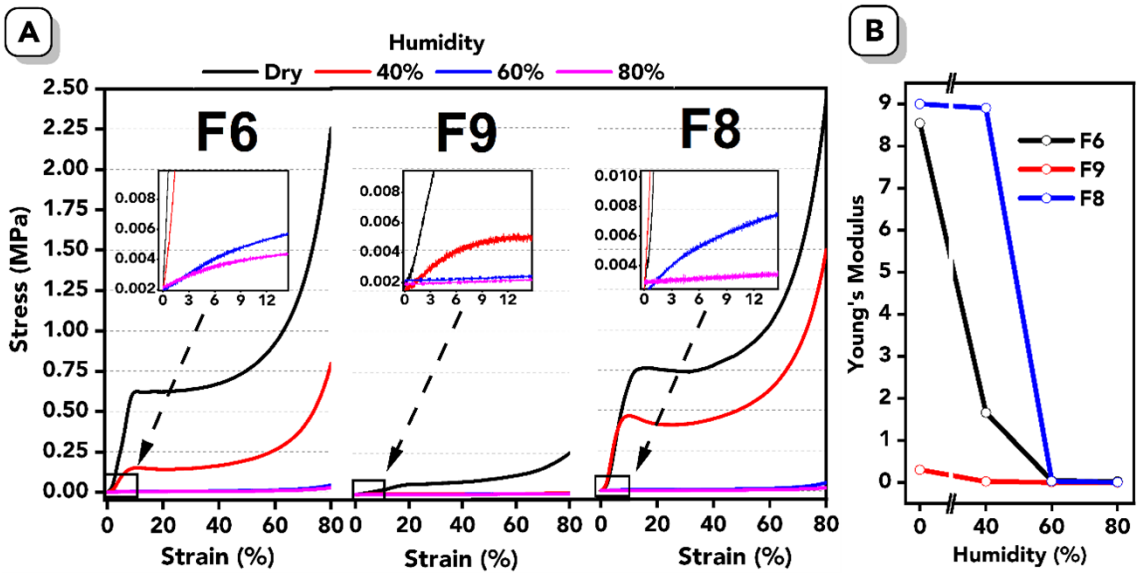

***Figure 11. A** - Stacked plots of stress vs. strain obtained in compression tests, performed on foams **F6**, **F9**, and **F8**, under different humidity, with a zoomed region; **B** - Stacked plots of Young's modulus humidity, (see **Table 1**, and **S2-3** in ESI for all formulations; section 6.3.3. for NIPUF synthesis conditions).*

3. Conclusions

This study introduces a novel approach to the production of non-isocyanate polyurethane foams (NIPUFs) via aminolysis chemistry, utilizing both simple (5CC) and exo-vinylene 5-membered (αCC) cyclic carbonates. Our method enables rapid foam generation at RT with tunable properties achieved by adjusting formulation variables such as the αCC-to-5CC ratio, water-to-5CC ratio, amine combinations, and the nature of αCC substituents. This approach provides, for the first time, polyhydroxyurethane foams bearing hydroxyoxazolidone (i.e., cyclic hydroxyurethane) pendant groups and does not require the utilization of epoxides in the formulation to reach the desired exotherm for foaming. Indeed, kinetic investigations show that the aminolysis of αCC is favored compared to its hydrolysis and is highly exothermic, which enables the selective production of

hydroxyoxazolidone moieties and induces the cascade exotherm needed to rapidly foam from RT formulations. The hydroxyurethane and vicinal diol moieties of the foams are produced by the aminolysis and hydrolysis of 5CC, respectively. The NIPUFs mechanical properties can be easily tailored over a wide range, delivering flexible to rigid foams through straightforward formulation adjustments (e.g., type and content of amines and αCCs, composition), a highly attractive feature inherent in the conventional PU foaming process. Although humidity impacts the foam's mechanical properties, our work lays a solid foundation for future advancements in NIPUF technology. The versatility and scalability of this approach open the door to new formulation possibilities, potentially expanding the range of applications for environmentally friendly polyurethane foams. This study not only showcases a novel and efficient pathway for full NIPU production but also addresses key formulation challenges, offering valuable insights for the development of next-generation 100% NIPUFs with improved performance and sustainability. Future research should focus on evaluating the toxicity of the primary NIPU formulation components. While the toxicity of common polyamines is generally well-documented and varies depending on their structure[46,47], the toxicity of 5CCs remains unexplored and warrants thorough investigation. Their higher boiling points, lower vapor pressures, and reduced reactivity compared to isocyanates suggest they may be safer to handle and less toxic. As for αCCs, their increased reactivity relative to conventional 5CCs raises the possibility of higher toxicity, but this has yet to be assessed.

4. Supporting Information

Supporting Information is available free of charge. Monomer synthesis procedures and foaming formulations, characterizations, FT-IR spectra, DSC and TGA thermograms, and ^{1}H and ^{13}C NMR spectra.

5. Acknowledgements

This is the authors' version of the article published in Macromolecules. Changes were made to this version by the publisher prior to publication. The final version is available at 10.1021/acs.macromol.4c02894

The authors are very grateful to CERM staff for technical assistance. C.D. is FNRS Research Director and thanks the "Fonds de la Recherche Scientifique (F.R.S.-FNRS) for funding. This work was realized in the frame of the WEL-T Advanced Grant financed by the Region Wallonne (FRFS-WEL-T; project "CHEMISTRY", convention WEL-T-CR-2023 A – 02) and CD thanks the Region Wallonne for funding. This technology is covered by patent application number EP24171055. This article was initially published as a preprint on ChemRxiv with the DOI: 10.26434/chemrxiv-2024-wnzpf.

6. Experimental part

6.1. Materials

The materials used in this study included: trimethylol propane triglycidyl ether (TMPTE, Aldrich, technical grade), Hydrotalcite synthetic ($Mg_6Al_2(CO_3)(OH)_{16}\cdot 4H_2O$, Aldrich), Potassium hydroxide (KOH, VWR International, 90%), 1-Heptylamine (Heptylamine, Thermo Scientific, 99+%), Propylene carbonate (PrC, Acros Organics BVBA, 99.5%), Tris(2-aminoethylamine) (TREN, Aldrich, 96%), m-Xylylene diamine (XDA, Aldrich, 99%), Isophorone diamine (IPDA, TCI, 98%), Jeffamine EDR-148 (TCI, 98%), Hexamethylene diamine (HMDA, Aldrich, 98%), 2-Methyl-3-butyn-2-ol (Aldrich, 98%), Silver carbonate (Merck, 99%), Triphenylphosphine (Aldrich, 99%), 1-Ethynyl-1-cyclohexanol (Themo Scientific, 99%), 3,5-Dimethyl-1-hexyn-3-ol (Aldrich, 99%), 2-Phenyl-3-butyn-2-ol (Aldrich, 99%), and Tetrabutylammonium iodide (TBAI, Aldrich, 99%).

6.2. Methods and Characterization

6.2.1. Gel Content (GC) Measurement

To determine the gel content, approximately 210 mg of each sample was weighed and incubated in glass vials containing around 30 mL of THF for 72 hours. The vials were shaken at 200 RPM on a VWR Micro Plate Shaker platform. Afterwards, the solution was removed from the vials, and vials with remaining foam samples were dried at 80 °C for 12 hours. The gel content was then calculated using the following equation:

$$\mathrm{GC} = \frac{(\text{weight of vial} + \text{sample } \mathbf{after} \text{ test}) - \text{weight of empty vial}}{(\text{weight of vial} + \text{sample } \mathbf{before} \text{ test}) - \text{weight of empty vial}} \times 100\%$$

6.2.2. Foam Density Calculation

The density of the foam was characterized in two ways. The total density of the entire foam sample was calculated by dividing its total mass by its calculated volume. Additionally, the average density of the foam's core was determined by measuring the volume and mass of 3-4 small cubes (approximately 1 cm x 1 cm x 1 cm) cut from different regions of the foam's core. The average inner foam density was obtained by dividing the average volume of these cubes by their average mass.

6.2.3. Fourier-Transform Infrared Spectroscopy (FT-IR)

A Nicolet IS5 spectrometer (Thermo Fisher Scientific) equipped with an attenuated total reflectance (ATR) accessory was used to obtain ATR-FTIR spectra of the inner part of foam samples. 32 scans were collected in the mid-infrared region (4000 - 550 cm^{-1}) with a resolution of 4 cm^{-1}. The resulting spectra were analyzed using OMNIA software (Thermo Fisher Scientific).

6.2.4. Nuclear Magnetic Resonance (NMR)

^{1}H-NMR and ^{13}C-NMR analyses were performed on a Bruker Avance 400 MHz spectrometer at 25°C. Deuterated solvents, such as chloroform-d ($CDCl_3$) or dimethyl sulfoxide-d_6 (DMSO-d_6), were used to prepare the samples for NMR analysis.

6.2.5. Differential Scanning Calorimetry (DSC)

Differential Scanning Calorimetry (DSC) was used to assess the thermal properties of the equilibrated foam samples. The foam samples, equilibrated at 25°C and 30% relative humidity for 72 hours in a Weisstechnik CareEvent climate chamber, were analyzed using a TA Instruments DSC250 calorimeter. A multi-step thermal cycling program was applied to ensure equilibration and to accurately determine the glass transition temperature (T_g). The temperature program consisted of three cycles with the following steps: Cooling from 25 °C to -50 °C at a rate of 5 °C/min, followed by a 2-minute isothermal hold at -50°C; heating from -40 °C to 80 °C at 5°C/min, followed by another 2-minute isothermal hold at 80°C. This cooling and heating procedure was repeated for two additional cycles to monitor the sample's equilibration. The first cycle was used to determine $T_{g,\,eq.}$ using TA Instruments' TRIOS software. Although the second cycle largely followed the same trend as the third, the third cycle was used for verification purposes as it reflected the thermal behavior of the foam under ensured dry conditions. In this cycle, the dry glass transition temperature ($T_{g,\,dry}$) was identified, with results calculated and interpreted using TRIOS software.

6.2.6. Thermogravimetric Analysis (TGA)

A Mettler Toledo TGA2 instrument was used to perform thermogravimetric analysis (TGA) on foam samples. Approximately 10 mg of each sample were dried overnight under vacuum at 80 °C. The measured dried foam samples were heated from 25 °C to 600 °C at a heating rate of 10°C/min under a nitrogen atmosphere (flow rate: 50 mL/min). The

degradation temperature at 5% weight loss ($T_{d5\%}$) was determined relative to the sample mass measured at 100°C to exclude the effect of any entrapped water.

6.2.7. Scanning Electron Microscopy (SEM)

The morphology of the foam was examined by first coating samples with a thin layer of platinum and then by using a FEI QUANTA 600 scanning electron microscope (SEM).

6.2.7. Compression Testing

The compression behavior of the foam was characterized by using the Instron 34TM-10 device with a cell force of 10 kN (for dry ***F6***, ***F9***, and ***F8*** samples and ***F6***, ***F8*** samples equilibrated at 40% humidity) or 500 N (for the ***F9*** sample equilibrated at 40% humidity and ***F6***, ***F9***, and ***F8*** samples equilibrated at 60% and 80% humidity). Bluehill Universal software was used for results evaluation.

Cubic foam samples with dimensions of 1.5 cm x 1.5 cm x 1.5 cm obtained from the core area of the foam with nearly identical density were equilibrated at a set humidity (40%/60%/80%) for 72 h in a Weisstechnik CareEvent climate chamber and compressed at a constant rate of 2 mm/min. The compression modulus was calculated from the slope of the stress-strain curve measured between different straight strains in the region of 2-12%.

6.3. Synthesis procedures

6.3.1. Synthesis of polyfunctional cyclic carbonates

TMPTC was prepared from TMPTE polyfunctional epoxide using the synthetic procedure mentioned in previous publications, including [29, 30, 35, 36].

6.3.2. Synthesis of activated cyclic carbonates (αCCs)

4,4-dimethyl-5-methylene-1,3-dioxolan-2-one (DMACC) was synthesized based on the procedure described at [42]. A detailed procedure is described in ***SI Section 4.*** MPACC, iBuMACC, and CHACC were prepared via the same method but using different precursors and adjusting pressure/temperature. All obtained products are described in ***SI Section 4, Figures S45-52.***

6.3.3. General procedure for NIPUF synthesis

The exact equivalent ratio, molar ratio, and masses for each formulation component can be found in **Table 1**, and **S2-3** in ESI.

In a 250 mL HDPE cylindrical cup, the poly(cyclic carbonate) was weighed with HTC and αCC, heated till 30 °C and mechanically stirred until a homogeneous mixture was obtained. In a separate glass vial, amine(s) were weighed (and stirred for homogeneity if applicable). In a second glass vial, a KOH solution in H_2O was prepared. A Matindale TT6K thermal probe was inserted 0.5 cm above the bottom of the HPDE cup and connected to the RS PRO 1384 recorder operated from D4IThermometer software. Amine and KOH solutions were simultaneously added into the HDPE cup and hand-stirred for 5 sec. A rapid exotherm with a following foam expansion occurred. The foam was cured for 20 min at RT.

Note that the exotherm might be significantly higher when higher volumes of formulations are used. As for the conventional self-blowing of polyurethane formulations, when other volumes of formulation are used for foaming, the formulation compositions

must be adapted to reach the desired exotherm and to avoid too vigorous exotherms that might lead to scorching or even fire.

7. References

[1] Gama, N. V.; Ferreira, A.; Barros-Timmons, A. Polyurethane Foams: Past, Present, and Future. Materials 2018, 11 (10), 1841. https://doi.org/10.3390/ma11101841.

[2] IAL consultant, 2018. Polyurethane chemicals and Product in Europe, Middle East and Africa, 2018.

[3] Seymour, R. B.; Kauffman, G. B. Polyurethanes: A class of modern versatile materials. J. Chem. Educ. 1992, 69 (11), 909. https://doi.org/10.1021/ed069p909.

[4] Peyrton, J.; Avérous, L. Structure-properties relationships of cellular materials from biobased polyurethane foams. Mater. Sci. Eng., R 2021, 145, 100608. https://doi.org/10.1016/j.mser.2021.100608.

[5] European Commission Regulation (EU) 2020/1149 of 3 August 2020 amending Annex XVII to Regulation (EC) No 1907/2006 of the European Parliament and of the Council concerning the Registration, Evaluation, Authorisation and Restriction of Chemicals (REACH) as regards diisocyanates. Official Journal of the European Union. 2020.

[6] U.S. Department of Labor, Occupational Safety and Health Administration. "Directive Number: CPL 03-00-017." National Emphasis Program – Occupational Exposure to Isocyanates. Effective Date: June 20, 2013. Last Modified: September 30, 2016.

[7] DHHS, Issues Related to Occupational Exposure to Isocyanates, 1989 to 2002, 2004.

[8] Rokicki, G.; Parzuchowski, P. G.; Mazurek, M. Non-isocyanate polyurethanes: synthesis, properties, and applications. Polym. Adv. Technol. 2015, 26 (7), 707–761. https://doi.org/10.1002/pat.3522.

[9] Maisonneuve, L.; Lamarzelle, O.; Rix, E.; Grau, E.; Cramail, H. Isocyanate-Free Routes to Polyurethanes and Poly(hydroxy Urethane)s. Chem. Rev. 2015, 115 (22), 12407–12439. https://doi.org/10.1021/acs.chemrev.5b00355.

[10] Cornille, A.; Auvergne, R.; Figovsky, O.; Boutevin, B.; Caillol, S. A perspective approach to sustainable routes for non-isocyanate polyurethanes. Eur. Polym. J. 2017, 87, 535–552. https://doi.org/10.1016/j.eurpolymj.2016.11.027.

[11] Kathalewar, M. S.; Joshi, P. B.; Sabnis, A. S.; Malshe, V. C. Non-isocyanate polyurethanes: from chemistry to applications. RSC Adv. 2013, 3, 4110–4129. https://doi.org/10.1039/C2RA21938G.

[12] Carré, C.; Ecochard, Y.; Caillol, S.; Avérous, L. From the Synthesis of Biobased Cyclic Carbonate to Polyhydroxyurethanes: A Promising Route towards Renewable Non-Isocyanate Polyurethanes. ChemSusChem 2019, 12 (15), 3410–3430. https://doi.org/10.1002/cssc.201900737.

[13] Ghasemlou, M.; Daver, F.; Ivanova, E. P.; Adhikari, B. Bio-based routes to synthesize cyclic carbonates and polyamines precursors of non-isocyanate polyurethanes: A review. Eur. Polym. J. 2019, 118, 668–684. https://doi.org/10.1016/j.eurpolymj.2019.06.032.

[14] Dros, A. B.; Larue, O.; Reimond, A.; De Campoa, F.; Pera-Titus, M. Hexamethylenediamine (HMDA) from fossil- vs. bio-based routes: an economic and life cycle assessment comparative study. Green Chem. 2015, 17, 4760–4772. https://doi.org/10.1039/C5GC01549A.

[15] Scodeller, I.; Mansouri, S.; Morvan, D.; Muller, E.; de Oliveira Vigier, K.; Wischert, R.; Jérôme, F. Synthesis of Renewable meta-Xylylenediamine from Biomass-Derived Furfural. Angew. Chem. 2018, 130 (33), 10670–10674. https://doi.org/10.1002/ange.201803828.

[16] Press release by EVONIK, "Evonik launches first renewable isophorone-based products", 2022.

[17] Cornille, A.; Blain, M.; Auvergne, R.; Andrioletti, B.; Boutevin, B.; Caillol, S. A Study of Cyclic Carbonate Aminolysis at Room Temperature: Effect of Cyclic Carbonate Structures and Solvents on Polyhydroxyurethane Synthesis. Polym. Chem. 2017, 8, 592–604. https://doi.org/10.1039/C6PY01854H.

[18] Blattmann, H.; Lauth, M.; Mülhaupt, R. Flexible and Bio-Based Nonisocyanate Polyurethane (NIPU) Foams. Macromol. Mater. Eng. 2016, 301 (8), 944–952. https://doi.org/10.1002/mame.201600141.

[19] Grignard, B.; Thomassin, J.-M.; Gennen, S.; Poussard, L.; Bonnaud, L.; Raquez, J.-M.; Dubois, P.; Tran, M.-P.; Park, C. B.; Jerome, C.; Detrembleur, C. CO_2-blown microcellular non-isocyanate polyurethane (NIPU) foams: from bio- and CO_2-sourced monomers to potentially thermal insulating materials. Green Chem. 2016, 18, 2206–2215. https://doi.org/10.1039/C5GC02723C.

[20] Datta-Sarma, A.; Zubkevich, S. V.; Addiego, F.; Schmidt, D. F.; Shaplov, A. S.; Berthé, V. Synthesis of High-Tg Nonisocyanate Polyurethanes via Reactive Extrusion and Their Batch Foaming. Macromolecules 2024, 57 (7), 3423–3437. https://doi.org/10.1021/acs.macromol.4c00222.

[21] Dong, T.; Dheressa, E.; Wiatrowski, M.; Prates-Pereira, A.; Zeller, A.; Laurens, L. M. L.; Pienkos, P. T. Assessment of Plant and Microalgal Oil-Derived Nonisocyanate Polyurethane Products for Potential Commercialization. ACS Sustainable Chem. Eng. 2021, 9, 38, 12858–12869. https://doi.org/10.1021/acssuschemeng.1c03653.

[22] Amezúa-Arranz, C.; Santiago-Calvo, M.; Rodríguez-Pérez, M. Á. A new synthesis route to produce isocyanate-free polyurethane foams. Eur. Polym. J. 2023, 197, 112366. https://doi.org/10.1016/j.eurpolymj.2023.112366.

[23] Cornille, A.; Dworakowska, S.; Bogdal, D.; Boutevin, B.; Caillol, S. A new way of creating cellular polyurethane materials: NIPU foams. Eur. Polym. J. 2015, 66, 129–138. https://doi.org/10.1016/j.eurpolymj.2015.01.034.

[24] Cornille, A.; Guillet, C.; Benyahya, S.; Negrell, C.; Boutevin, B.; Caillol, S. Room temperature flexible isocyanate-free polyurethane foams. Eur. Polym. J. 2016, 84, 873–888. https://doi.org/10.1016/j.eurpolymj.2016.05.032.

[25] Coste, G.; Berne, D.; Ladmiral, V.; Negrell, C.; Caillol, S. Non-isocyanate polyurethane foams based on six-membered cyclic carbonates. Eur. Polym. J. 2022, 176, 111392. https://doi.org/10.1016/j.eurpolymj.2022.111392.

[26] Coste, G.; Denis, M.; Sonnier, R.; Caillol, S.; Negrell, C. Synthesis of reactive phosphorus-based carbonate for flame retardant polyhydroxyurethane foams. Polym. Degrad. Stab. 2022, 202, 110031. https://doi.org/10.1016/j.polymdegradstab.2022.110031.

[27] Clark, J. H.; Farmer, T. J.; Ingram, I. D. V.; Lie, Y.; North, M. Renewable Self-Blowing Non-Isocyanate Polyurethane Foams from Lysine and Sorbitol. Eur. J. Org. Chem. 2018, 31, 4265–4271. https://doi.org/10.1002/ejoc.201800665.

[28] Choong, P. S.; Hui, Y. L. E.; Lim, C. C. CO2-Blown Nonisocyanate Polyurethane Foams. ACS Macro Lett. 2023, 12 (8), 1094–1099. https://doi.org/10.1021/acsmacrolett.3c00334.

[29] Monie, F.; Grignard, B.; Thomassin, J. M.; Mereau, R.; Tassaing, T.; Jerome, C.; Detrembleur, C. Chemo- and Regioselective Additions of Nucleophiles to Cyclic Carbonates for the Preparation of Self-Blowing Non-Isocyanate Polyurethane Foams. Angew. Chem. Int. Ed. 2020, 59 (39), 17033–17041. https://doi.org/10.1002/anie.202006267.

[30] Monie, F.; Grignard, B.; Detrembleur, C. Divergent Aminolysis Approach for Constructing Recyclable Self-Blown Nonisocyanate Polyurethane Foams. ACS Macro Lett. 2022, 11 (2), 236–242. https://doi.org/10.1021/acsmacrolett.1c00793.

[31] Coste, G.; Negrell, C.; Caillol, S. Cascade (Dithio)carbonate Ring Opening Reactions for Self-Blowing Polyhydroxythiourethane Foams. Macromol. Rapid Commun. 2022, 43 (13), 2100833. https://doi.org/10.1002/marc.202100833.

[32] Purwanto, N. S.; Chen, Y.; Wang, T.; Torkelson, J. M. Rapidly synthesized, self-blowing, non-isocyanate polyurethane network foams with reprocessing to bulk networks via hydroxyurethane dynamic chemistry. Polymer 2023, 272, 125858. https://doi.org/10.1016/j.polymer.2023.125858.

[33] Purwanto, N. S.; Chen, Y.; Torkelson, J. M. Biobased, reprocessable, self-blown non-isocyanate polyurethane foams: influence of blowing agent structure and functionality. Eur. Polym. J. 2024, 206, 1127775. https://doi.org/10.1016/j.eurpolymj.2024.112775.

[34] Chen, Y.; Purwanto, N. S.; Chen, B.; Wang, T.; Kim, S.; Huang, Y.; Ditchel, W. R.; Torkelson, J. M. Biobased, catalyst-free non-isocyanate polythiourethane foams: highly dynamic nature affords fast reprocessability, extrudability, and refoamability. Chem. Eng. J. 2024, 496, 154035. https://doi.org/10.1016/j.cej.2024.154035.

[35] Bourguignon, M.; Grignard, B.; Detrembleur, C. Water-Induced Self-Blown Non-Isocyanate Polyurethane Foams. Angew. Chem. Int. Ed. 2022, 61 (51), e202213422. https://doi.org/10.1002/anie.202213422.

[36] Bourguignon, M.; Grignard, B.; Detrembleur, C. Cascade Exotherms for Rapidly Producing Hybrid Nonisocyanate Polyurethane Foams from Room Temperature Formulations. J. Am. Chem. Soc. 2024, 146 (1), 988–1000. https://doi.org/10.1021/jacs.3c11637.

[37] Gennen, S.; Grignard, B.; Tassaing, T.; Jérôme, C.; Detrembleur, C. CO2-Sourced α-Alkylidene Cyclic Carbonates: A Step Forward in the Quest for Functional Regioregular Poly(urethane)s and Poly(carbonate)s. Angew. Chem. Int. Ed. 2017, 56 (35), 10394–10398. https://doi.org/10.1002/anie.201704467.

[38] Tounzoua, C. N.; Grignard, B.; Detrembleur, C. Exovinylene Cyclic Carbonates: Multifaceted CO2-Based Building Blocks for Modern Chemistry and Polymer Science.

Angewandte Chemie 2022, 61(22), e202116066. https://doi.org/10.1002/anie.202116066.

[39] Habets, T.; Olmedo-Martínez, J. L.; del Olmo, R.; Grignard, B.; Mecerreyes, D.; Detrembleur, C. Facile Access to CO2-Sourced Polythiocarbonate Dynamic Networks and Their Potential As Solid-State Electrolytes For Lithium Metal Batteries. ChemSusChem 2023, 16(14), e202300225. https://doi.org/10.1002/cssc.202300225.

[40] Siragusa, F.; Demarteau, J.; Habets, T.; Olazabal, I.; Robeyns, K.; Evano, G.; Mereau, R.; Tassaing, T.; Grignard, B.; Sardon, H.; Detrembleur, C. Unifying Step-Growth Polymerization and On-Demand Cascade Ring-Closure Depolymerization via Polymer Skeletal Editing. Macromolecules 2022, 55(11), 4637–4646. https://doi.org/10.1021/acs.macromol.2c00696.

[41] Razavi-Esfali, M.; Habets, T.; Siragusa, F.; Grignard, B.; Sardon, H.; Detrembleur, C. Design of functional isocyanate-free poly(oxazolidone)s under mild conditions. Polymer Chemistry 2024, 15, 1962–1974. https://doi.org/10.1039/D4PY00101J.

[42] Habets, T.; Siragusa, F.; Grignard, B.; Detrembleur, C. Advancing the Synthesis of Isocyanate-Free Poly(oxazolidones)s: Scope and Limitations. Macromolecules 2020, 53(15), 6396–6408. https://doi.org/10.1021/acs.macromol.0c01231.

[43] Boult, M. A.; Gamadia, R. K.; Napier, D. H. Thermal Degradation of Polyurethane Foams. IChemE Symposium Series 1970, 33.

[44] Amado, J. C. Q. Thermal Resistance Properties of Polyurethanes and Its Composites. Thermosoftening Plastics IntechOpen, 2020, 87039.

[45] Peng, H.-K.; Wang, X. X.; Li, T.-T.; Huang, S.-Y.; Lin, Q.; Shiu, B.-C.; Lou, C.-W.; Lin, J.-H. Effects of hydrotalcite on rigid polyurethane foam composites containing a fire retarding agent: compressive stress, combustion resistance, sound absorption, and electromagnetic shielding effectiveness. RSC Adv. 2018, 8, 33542–33550. https://doi.org/10.1039/C8RA06361C.

[46] Bergeron, R. J.; Feng, Y.; Weimar, W. R.; McManis, J. S.; Dimova, H.; Porter, C.; Raisler, B.; Phanstiel, O. A Comparison of Structure−Activity Relationships between Spermidine and Spermine Analogue Antineoplastics. J. Med. Chem. 1997, 40 (10), 1475–1494. https://doi.org/10.1021/jm960849j.

[47] Pegg, A. E. Toxicity of Polyamines and Their Metabolic Products. Chem. Res. Toxicol. 2013, 26 (12), 1782–1800. https://doi.org/10.1021/tx400316s.